Applied Catalysis B: Environmental 199 (2016) 252–259

Contents lists available at ScienceDirect

Applied Catalysis B: Environmental

journal homepage: www.elsevier.com/locate/apcatb

Quantitative screening of an extended oxidative coupling of methane catalyst library

V.I. Alexiadis[a], M. Chaar[b], A. van Veen[b,1], M. Muhler[b], J.W. Thybaut[a,*], G.B. Marin[a]

[a] Laboratory for Chemical Technology, Ghent University, Technologiepark 914, B-9052, Ghent, Belgium
[b] Laboratory of Industrial Chemistry, Department of Chemistry, Ruhr-University Bochum, D-44780, Bochum, Germany

ARTICLE INFO

Article history:
Received 6 March 2016
Received in revised form 19 May 2016
Accepted 4 June 2016
Available online 6 June 2016

Keywords:
Ethylene
Homogeneous-heterogeneous reaction network
Alkaline earth catalyst
NaMnW catalyst
Microkinetic modelling
LiMgO catalyst

ABSTRACT

A comprehensive microkinetic model, including catalyst descriptors, that accounts for the homogeneous as well as heterogeneously catalyzed reaction steps in Oxidative Coupling of Methane (OCM) was used in the assessment of large kinetic datasets acquired on five different catalytic materials. The applicability of the model was extended from alkali magnesia catalysts represented by Li/MgO and Sn-Li/MgO and alkaline earth lanthana catalysts represented by Sr/La_2O_3 to rare earth-promoted alkaline earth calcium oxide catalysts, represented by LaSr/CaO, and to a $Na\text{-}Mn\text{-}W/SiO_2$ catalyst. The model succeeded in adequately simulating the performance of all five investigated catalysts in terms of reactant conversion and product selectivities in the entire range of experimental conditions. It was found that the activity of Sr/La_2O_3, in terms of methane conversion, is approximately 2, 5, 30 and 33 times higher than over the La-Sr/CaO, Sn-Li/MgO, $Na\text{-}Mn\text{-}W/SiO_2$ and Li/MgO catalysts, respectively, under identical operating conditions. This was attributed mainly to the high stability of adsorbed hydroxyls, the high stability of adsorbed oxygen and the high concentration of active sites of Sr/La_2O_3. The selectivity towards C_2 products was found to depend on the methyl radical sticking coefficient and the stability of the adsorbed oxygen and was the highest on the $Na\text{-}W\text{-}Mn/SiO_2$ catalyst, that is 75% at about 1% methane conversion and 1023 K, 190 kPa and inlet molar CH_4/O_2 ratio of 4.

1. Introduction

Oxidative coupling of methane (OCM) to ethylene has been studied for more than 30 years [1] and offers significant industrial potential, since it could broaden the feedstock basis for the chemical industry. The production of ethylene from natural gas represents a significant opportunity because of its massive, worldwide use as a monomer in plastics production. Furthermore, ethylene can be oligomerized into liquid hydrocarbons, such as alpha olefins or gasoline, thereby enabling the efficient utilization of natural gas in so-called stranded areas [2]. At present, ethylene is mainly produced by steam cracking of naphtha, a crude oil product. The importance of alternative carbon sources becomes greater as oil price increases as well as in view of sustainability [3].

OCM can be described as a gas phase reaction which is initiated via heterogeneous catalysis [4]. The catalyst is activated through reversible, dissociative oxygen chemisorption resulting in surface oxygen species that provoke gas phase methyl radical formation by hydrogen abstraction from methane. The formed methyl radicals either couple in the gas phase to form C_2 products or are oxidized towards carbon oxides [5,6]. Several metal oxides have been investigated thoroughly for this reaction, some of which proved to be effective catalysts, such as lithium magnesia catalysts, alkaline earth lanthana catalysts, rare earth-promoted alkaline earth calcium oxide catalysts and $Na\text{-}Mn\text{-}W/SiO_2$ catalysts. However, none of them has reached the stage of commercial implementation yet, since their performance in terms of C_2 yield remains relatively low [5].

An elaborate microkinetic model for OCM, that includes catalyst descriptors and accounts for thermal, homogeneous and catalytic, heterogeneous reaction steps has been developed aiming at fine tuning the best catalytic materials [5,7]. Model parameters such as reaction enthalpies and activation energies have been related to selected chemisorption enthalpies. The latter are denoted as catalyst descriptors and the established relationships between these descriptors and the model parameters have been constructed to be valid for an entire catalyst library. A more detailed description of the OCM microkinetic model is presented by Kechagiopoulos

* Corresponding author.
E-mail address: Joris.Thybaut@UGent.be (J.W. Thybaut).
[1] Present address: University of Warwick, School of Engineering, Coventry, CV 7AL, UK.

http://dx.doi.org/10.1016/j.apcatb.2016.06.019

Nomenclature

Roman

E_0	Reference activation energy of a reaction family, kJ/mol
$F^{\circ}_{reactants}$	Inlet flow rate of reactants (CH_4 and O_2), mol/s
rf_i	Reaction family i
S_i	Selectivity towards product i, %
W	Catalyst mass, kg
X_i	Conversion of reactant i, %
F_{feed}	Total flow rate of the reactor feed, mol/s
p	Pressure, kPa
T	Temperature, K

Greek

α	Transfer coefficient of a reaction family

et al. [7], offering an insight into the actual model construction, the OCM reaction pathways on which the model is based and the intra-particle concentration profiles of the surface species included in the model. The recent study of Alexiadis et al. [5] focuses on the ability of the model to assess OCM kinetic data acquired on catalysts that are representative of two different classes of materials, that are lithium magnesia and alkaline earth-promoted lanthana catalysts, and associate their performance in terms of methane activation and C_2 selectivity to selected catalyst descriptors.

In the present work, the model's applicability beyond the previously used catalyst classes is demonstrated, that is for rare earth-promoted alkaline earth calcium oxide catalysts, represented by LaSr/CaO, and Na-Mn-W/SiO_2 catalysts. Thanks to the model, an unequivocal and quantified comparison of these OCM catalyst classes comes within reach. The implementation of the microkinetic model for a series of catalysts belonging to the same class being rather straightforward, a similar effort for catalysts belonging to different classes is significantly more challenging.

2. Procedures

2.1. Experimental

Extensive OCM experimental datasets were acquired over a 10%La-20%Sr/CaO and a 1wt%Na-3%W-2%Mn/SiO_2 catalyst covering a wide range of operating conditions complementary to the previously acquired data on the Li/MgO, Sn-Li/MgO and Sr/La_2O_3 catalysts. Perovskite catalysts have also been considered [8,9] but appeared to be severely affected by Cr diffusion when deposited on a stainless steel microreactor [10] and, hence, have been discarded in the present work. In what follows, a brief description is given of the LaSr/CaO and NaWMn/SiO_2 catalytic materials, the experimental set up and the employed operating conditions during the OCM experiments. Materials and procedures for the acquisition of literature data on Li/MgO, Sn-Li/MgO and Sr/La_2O_3 performances [5,11,12] are provided alongside for reference.

2.1.1. Catalysts

Rare earth-promoted alkaline earth calcium oxide catalytic systems have only been investigated to a limited extent [13,14] although they are recognized as highly performing and stable OCM catalysts. It has been reported that CaO is a high temperature stable, basic catalyst support with La being involved in the oxygen activation and Sr enhancing the C_2 selecticity. Within the present study, the catalyst 10%La – 20%Sr/CaO was selected to be investigated more elaborately given the promising perspectives from preliminary data [13].

Na-W-Mn/SiO_2 catalysts constitute one of the few classes that have been investigated extensively in the OCM reaction, but for which no fundamental model had been developed yet [15–21]. Their catalytic performance at moderate temperature and stability over extended time on stream has been reported by several research groups.

The latter is further enhanced when they have been prepared via the wet impregnation method [15,16]. Despite the extensive research on this catalyst class, a detailed interpretation of the fundamental phenomena at the origin of its performance is not available. Within the current investigation, a catalyst with composition 1wt%Na-3%W-2%Mn/SiO_2 was selected, which is identical to a literature reported catalyst in terms of preparation method and composition [16].

Table 1a presents the main structural properties of these two catalysts in comparison to previously investigated Sr/La_2O_3 and the MgO based catalysts [6]. As can be easily observed, the investigated catalysts present roughly similar physical properties allowing to focus on the differences in chemical properties. The low values of the surface area of the catalysts are in line with previous findings [13,16,22].

2.1.2. Set up

The experimental data over LaSr/CaO and NaMnW/SiO_2 were obtained in a fixed bed reactor, operating in the plug-flow regime with minimal axial and radial temperature gradients and negligible pressure drop over the catalyst bed. These conditions justify the use of a one-dimensional reactor model in the simulation of the experimental data using the OCM microkinetic model. Further information on the set-up has been previously reported [5].

2.1.3. Operating conditions

The reproducibility of the kinetic measurements was ensured by applying a standardized lining-out pretreatment for both catalysts, identical to the one previously applied for the Sr/La_2O_3 catalyst [5]. The concentration of reactive gas was maintained below 70% for safety reasons in the set-up used in the present work.

Variable parameters were the inlet molar ratio of CH_4:O_2, the space time which was calculated based on the sum of both reactant inlet flow rates, that is CH_4 and O_2, the dilution of the reactive gas and the catalyst temperature, see also Table 1b. High reactant flow rates were used to avoid external mass transfer limitations to the largest possible extent, see further. The maximum employed catalyst mass was set at 350 mg to keep oxygen conversion below 90%. The corresponding space times were defined accordingly. Catalyst temperatures were kept below 900 °C to ensure long term stabil-

Table 1a
Physical properties of the investigated catalysts.

Property	Sr/La_2O_3	LaSr/CaO	NaMnW/SiO_2	Li/MgO	Sn-Li/MgO
Radius of catalyst pellet (mm)	0.1	0.1	0.1	0.125	0.125
Surface area (m^2/g)	2	4.7	2.3	1	2.8
Pore volume (cm^3/g)	0.024	0.04	0.004	–	–
Porosity ($m_g^3\ m_c^{-3}$)	0.27	0.27	0.27	0.29	0.27
Density (kg m_c^{-3})	2300	2600	2300	2350	2300

Table 1b
Operating conditions employed over the investigated catalysts.

Operating condition	[a]Sr/La_2O_3	LaSr/CaO	$NaMnW/SiO_2$	[a](Sn-)Li/MgO
Pressure (kPa)	190	190	120	108–130
Temperature (K)	980–1180	950–1180	1012–1085	947–1013
CH_4/O_2 ($mol_{CH4}\ mol_{O2}^{-1}$)	2–4	2–4	1–6	2–12
$W/F_{reactants}$ ($kg\ s\ mol_{reactants}^{-1}$)	0.2–1.2	0.3–0.8	3–25	2–12
N_2 dilution (%)	80	50–80	30–80	0
Catalyst loading (mg_c)	15–75	50	250–350	375

[a] according to previously acquired experimental data [5,11,12].

ity in the kinetic experimentation. Extensive kinetic datasets were compiled over LaSr/CaO and $NaMnW/SiO_2$ catalysts comprising 157 and 228 observations respectively. The operating conditions previously used for the acquisition of the OCM kinetics data on Sr/La_2O_3, Li/MgO and Sn-Li/MgO [5,11,12] are provided in Table 1b alongside for reference.

2.2. Model simulations

The OCM microkinetic model was in the first instance validated against the experimental data produced over the LaSr/CaO and the $NaMnW/SiO_2$ catalysts. Below is a brief discussion of the model characteristics as required for the proper understanding of the current work. A more elaborate description of the model has been reported elsewhere [5,7].

2.2.1. Reaction kinetics

The gas phase reaction network of the microkinetic model has been developed in terms of 39 elementary steps [5–7,11,12,14,23]. The catalytic reaction network comprises 26 elementary steps [5,7] which can be classified into three types, that are adsorption steps, Eley-Rideal reactions and surface reactions [5].

2.2.2. Reactor model

The microkinetic model was implemented in a one-dimensional, heterogeneous reactor model, which explicitly accounts for the irreducible mass transport limitations induced by the high reactivity of the produced radicals. It also accounts for the diluent effect on the relative contribution to the overall conversion by heterogeneous and homogeneous reactions due to a changing available gas phase and catalyst surface in the catalyst bed. A more detailed description of the reactor model has been given by Kechagiopoulos et al. [7].

2.2.3. Model parameters

The rate coefficients of the catalytic steps were calculated from the respective pre-exponential factors and activation energies. The maximum value of the pre-exponential factors of the steps involving interaction of a gas phase species with the catalyst surface [6,24], that is the adsorption and the Eley-Rideal steps, was estimated by collision theory. The pre-exponential factors for the adsorption steps were corrected with separate initial sticking probabilities (S_0) which were considered as catalyst descriptors in the microkinetic model. The pre-exponential factor values for the surface reaction steps were determined by transition-state theory.

The activation energies of the catalytic steps were calculated from the surface thermodynamics via Polanyi relationships. Surface thermodynamics in turn were obtained from the catalyst descriptors by applying thermodynamic consistency through the considered catalytic cycles. This allowed expressing reaction enthalpies for various elementary steps as a function of a limited number of unknown catalyst descriptors which are subsequently estimated by regression [6,25,26].

All adsorption steps were considered to be non-activated. As shown in Table 2, the Eley-Rideal steps were grouped into a single reaction family (rf1), while the surface reaction steps were subdivided into four reaction families, accounting for H-atom abstraction (rf2), recombination of hydroxyls (rf3), catalytic oxidation of CO (rf4) and C–C bond scission (rf5) respectively. Each reaction family (rf1–rf5) has a specific set of Polanyi parameters α and E_0. Values of α were taken from literature [27–30]. The reference activation energies, E_0, were defined as kinetic descriptors and their values during regression analysis were fixed at the values obtained during the parameter adjustment over the Sr/La_2O_3 data [5].

The set of catalyst descriptors in the OCM microkinetic model can be classified as follows:

a) Reaction enthalpy of hydrogen abstraction from CH_4 (D_1).
b) Chemisorption heats of O_2, CH_2O, HCO, CO, CO_2, H_2O, C_2H_4O, C_2H_3O (D_2-D_9).
c) Initial sticking probabilities of O_2, CH_3, CO, CO_2, H_2O, C_2H_4 (D_{10}–D_{15}).
d) Density of active sites (D_{16}).

As shown in our previous work [5] a more pronounced endothermicity of hydrogen abstraction from methane, that is a higher D1, results in an equivalent decrease of the hydroxyl stability on the catalyst surface. The stability of the hydroxyl species influences the methane activation and the C_2 selectivity, mainly via the formation of adsorbed atomic oxygen.

2.2.4. Parameter estimation

Parameter estimation was performed using the Rosenbrock methodology [31] for the initial minimization of the objective function, that is the weighed sum of the squared residuals, followed by a Levenberg–Marquardt algorithm [32] for the final optimization. Further information on parameter estimation procedure is given elsewhere [5]. As discussed in Section 2.2.3, the estimated parameters are the catalyst and kinetic descriptors.

The initial guesses for the catalyst descriptors were chosen to be within the range of physically realistic values [5]. For example, the adsorption heat of CO, ranges between 60 and 180 KJ/mol [33], while the adsorption heat of water can reach up to 65 KJ/mol [34]. The molar fractions of methane, oxygen, ethylene, ethane, carbon monoxide and carbon dioxide at the reactor outlet were used as responses in the parameter estimation procedure.

Table 2
Reaction families and corresponding parameters employed in the Polanyi relationships considered in the model. Transfer coefficients, α, were obtained from the literature as indicated while reference activation energies were as determined in our previous work [5].

	Reaction family	α	E_0 (kJ/mol)
rf_1	Hydrogen abstraction by Eley-Rideal reaction	0.75 [27]	96.8
rf_2	Hydrogen abstraction by surface reaction	0.50 [28]	141.3
rf_3	Recombination of hydroxyls	0.65 [29]	130.2
rf_4	CO oxidation on the surface	0.26 [30]	67.6
rf_5	C–C cleavage on the surface	0.97 [30]	185.7

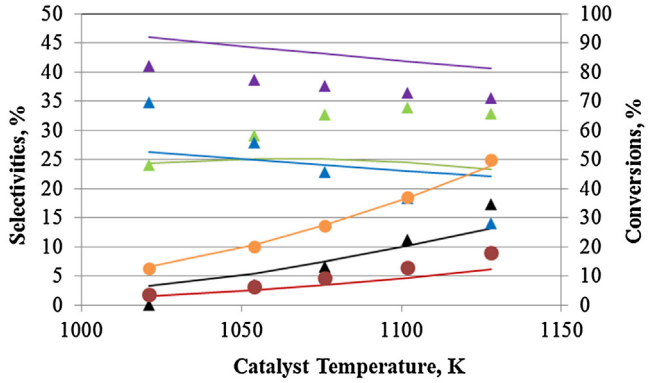

Fig. 1. Conversions and selectivities over La-Sr/CaO vs. catalyst temperature. Experimental conditions: p = 190 kPa, CH_4/O_2 = 3, N_2 dilution = 80%, W = 50 mg and F_{feed} = 3.08 10^{-4} mol/s. Symbols-experimental points: ● : CH_4 conversion, ● : O_2 conversion, ▲ : C_2H_6 selectivity, ▲: C_2H_4 selectivity, ▲ : CO selectivity, ▲ : CO_2 selectivity. Experimental points present same colour with the respective calculation curves. Calculated conversions and selectivities were produced with the model described in section 2 and the values of catalyst descriptors listed in Table 4.

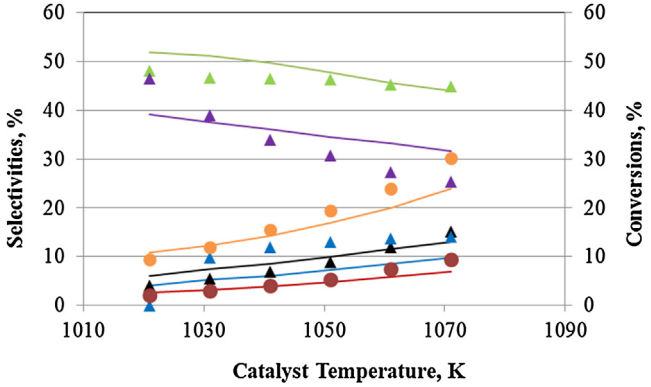

Fig. 2. Conversions and selectivities over Na-Mn-W/SiO_2 vs. catalyst temperature. Experimental conditions: p = 120 kPa, CH_4/O_2 = 4, N_2 dilution = 75% and W/F $_{reactants}$ = 19.5 kg s $mol^{-1}{}_{reactants}$. Symbols-experimental points: ● :CH_4 conversion, ● : O_2 conversion, ▲ : C_2H_6 selectivity, ▲: C_2H_4 selectivity, ▲ : CO selectivity, ▲ : CO_2 selectivity. Experimental points present same colour with the respective calculation curves. Calculated conversions and selectivities were produced with the model described in section 2 and the values of catalyst descriptors listed in Table 4.

3. Results and discussion

3.1. Experimental catalyst assessment

3.1.1. La-Sr/CaO

An extensive experimental data set comprising 157 points was acquired during OCM testing of the 10wt%La-20wt%Sr/CaO catalyst. As presented in Table 1b, during testing under OCM conditions, the catalyst temperature, the inlet CH_4/O_2 ratio and the N_2 dilution were varied. The latter determined the space time of the reactants, since the total gas feed inlet flow rate and the catalyst mass were fixed at 3.08 10^{-4} mol/s and 50 mg respectively. The stability of the catalyst was verified within a time on stream of 60 h without loss in activity or selectivity.

Fig. 1 depicts the effect of the catalyst temperature on the methane and oxygen conversion and major product selectivities at a N_2 dilution of 80% of the total feed. The total pressure and inlet molar methane to oxygen ratio were fixed at 190 kPa and 3 respectively. As expected, methane and oxygen conversions increase with the temperature. In particular, the methane conversion reaches 18% and that of oxygen reaches 50% at 1128 K. As shown in Fig. 1, the C_2 selectivity, that is ethane and ethylene, increases with the catalyst temperature. The ethane selectivity reaches a maximum of 34% at 1100 K while that of ethylene is more temperature dependent and increases monotonically to reach 17.5% at 1128 K. As in the case of Sr/La_2O_3 described elsewhere [5], the selectivity towards carbon oxides decreases with temperature, with the CO selectivity being more temperature-dependent dropping down to 15% at 1128 K.

3.1.2. Na-Mn-W/SiO_2

A dataset comprising 228 observations was produced over 1 wt%Na-3 wt%W-2 wt% Mn/SiO_2 by varying the catalyst temperature, the inert gas dilution, the space time and the inlet molar CH_4/O_2 ratio. The total pressure was again fixed at 120 kPa. Catalyst stability was verified within a time on stream of 60 h as in the case of LaSr/CaO.

Fig. 2 presents the effect of the catalyst temperature on the methane and oxygen conversion and selectivities towards C_2 and CO_x by keeping N_2 dilution, space time, and inlet CH_4/O_2 ratio constant at 75%, 19.5 kg s $mol^{-1}{}_{reactants}$ and 4 respectively. As expected, methane and oxygen conversions increase with the temperature, reaching a maximum of 9.5% and 30.3% respectively at 1071 K under the investigated experimental conditions. As shown in Fig. 2, the ethane selectivity slightly decreases with the temperature at these conditions while the ethylene selectivity increases monotonically with increasing temperature reaching 15.1% at 1071 K. The CO_2 selectivity decreases considerably with the temperature, while that towards CO is practically zero up to 1020 K and subsequently increases.

3.1.3. Comparison of the OCM behaviour of the investigated catalysts

In our previous work [5] extensive OCM kinetic data of 30, 40 and 176 experimental points produced over Li/MgO, Sn-Li/MgO and Sr/La_2O_3 catalyst respectively, were employed for assessing the performance of an alkali manganese catalyst, its Sn promoted version and an alkaline earth-promoted lanthana catalyst. Note that a significantly wider range of space times was used on the (Sn-)Li/MgO and the NaMnW/SiO_2 catalysts compared to Sr/La_2O_3 and LaSr/CaO catalysts, see also Table 1b.

Performances of the above five catalysts were compared in terms of methane conversion and C_2 selectivity. Representative experimental results are presented in Table 3. All the experimental data have been acquired at a catalyst temperature of approximately 1020 K. The applied methane to oxygen inlet ratio of 3.5 was slightly lower in the case of Sn-Li/MgO, compared to the other four catalysts, for which a ratio of 4 was employed. Moreover, the total pressure was close to atmospheric in the cases of NaMnW/SiO_2 and Li-based MgO catalysts, while it was slightly higher in the case of Sr/La_2O_3 and LaSr/CaO catalyst, that is 190 kPa. During the experiments over the Li-based MgO catalysts, there was no dilution of the feed reactive gas, while for the other catalysts the experiments were conducted under high inert gas (N_2) dilution, that is 75–80%.

It is clear from Table 3 that Li/MgO and Na-Mn-W/SiO_2, by far, are the least active catalysts. In particular, the latter catalyst exhibits a low activity even when relatively high space times are employed. Sr/La_2O_3 is more active and slightly less selective than La-Sr/CaO at similar operating conditions. The Sn-Li/MgO catalyst was investigated at much more concentrated conditions, higher reactant space times and a slightly lower CH_4/O_2 ratio. All above aspects are expected to promote methane conversion. As seen in Table 3, the Sn-Li/MgO catalyst presents the highest C_2 selectivity value, yet this value corresponds to the highest methane conversion among the investigated catalysts reported in this table. A concrete comparison of catalysts in terms of C_2 selectivity should refer to the same methane conversion, see also Section 3.3. The assessment of the data making use of a microkinetic model allows

Table 3
Typical OCM performance of the investigated catalysts.

Catalyst	Space time, kg s mol$^{-1}_{reactants}$	CH_4/O_2	Feed dilution, %	Catalyst T, K	p, kPa	X CH_4, %	S C_2, %
Sr/La_2O_3	0.8	4	80	1023	190	7	23.4
La-Sr/CaO	0.8	4	80	1020	190	3.2	26.7
Na-Mn-W/SiO_2	19.5	4	75	1021	120	2.1	52.5
Li/MgO	4	4	0	1023	112	0.9	49
Sn-Li/MgO	2	3.5	0	1023	117	12.4	58.1

efficiently accommodating these differences in operating conditions and quantifies the catalyst performance in terms of catalyst descriptors, which allow an unequivocal comparison of the considered catalysts.

3.2. Extending the microkinetic model validity to LaSr/CaO and NaMnW/SiO_2

The microkinetic model used in the present work had already been validated against the data acquired on the Sr/La_2O_3 and the MgO-based catalysts [5]. The experimental data produced over LaSr/CaO and NaMnW/SiO_2 catalysts have now also been simulated making use of this model to quantify the distinct activity and selectivity patterns in the performance of these two investigated catalysts, see Fig. 1 and 2 compared to the previously investigated ones. As reported in our previous work [5], the microkinetic model is most sensitive to the following four catalyst descriptors: the H-atom abstraction enthalpy from methane (D_1), the chemisorption heat of oxygen (D_2), the initial sticking probability of CH_3 radicals on the surface (D11) and the active site density (D_{16}). During the regression analysis, only the four aforementioned descriptors, D_1, D_2, D_{11} and D_{16}, see Table 4, were allowed to vary. The values of the remaining catalyst and kinetic descriptors, were fixed at the values obtained, during the parameter estimation performed for the Sr/La_2O_3 data [5].

Reduced datasets of 36 and 43 experiments for the LaSr/CaO and NaMnW/SiO_2 catalyst respectively were used in the parameter estimation procedure in order to reduce the computational time. The estimated catalyst descriptor values were then validated against all 157 and 228 observations on each of the investigated catalysts. Fig. 3a and b present the parity diagrams for CH_4, O_2 and C_2 products.

As can be clearly seen from Fig. 3a and b, the microkinetic model yielded a very good agreement with the experimental data for the

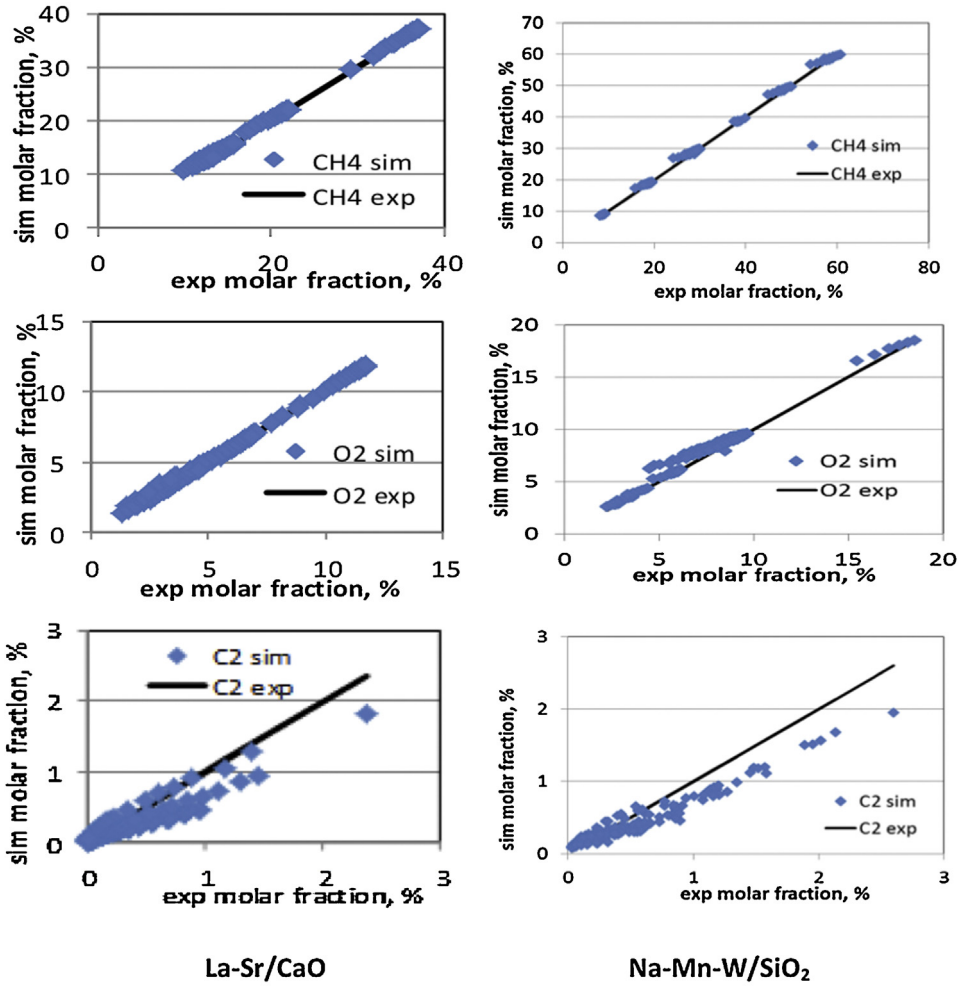

Fig. 3. Parity diagrams for CH_4, O_2 and C_2 (ethane + ethylene) over the catalysts La-Sr/CaO and Na-Mn-W/SiO_2. The experimental conditions are summarised in Tables 1a and 1b. Modelling results were obtained with the model described in section 2 and the values of catalyst descriptors listed in Table 4.

Table 4
Catalyst descriptor estimates as obtained by regression of the microkinetic model reported by Alexiadis et al. [5] to the experimental data obtained on La-Sr/CaO and Na-Mn-W/SiO_2. Previously reported values for Sr/La_2O_3, Li/MgO and Sn-Li/MgO [5] are included for easy comparison.

	Catalyst descriptor	Unit	La-Sr/CaO	Na-Mn-W/SiO_2	Sr/La_2O_3	Li/MgO	Sn-Li/MgO
D_1	Reaction enthalpy of hydrogen abstraction from CH_4	(kJ mol^{-1})	65.1 ± 1.6	81.4 ± 0.002	44.4 ± 0.2	91.2 ± 0.2	56.6 ± 0.8
D_2	Chemisorption heat of O_2	(kJ mol^{-1})	139.6 ± 5.3	44 ± 1.6	119.5 ± 3.5	73.6 ± 2.2	60.54 ± 2.6
D_{11}	Initial sticking probability of CH_3·		1.14 ± 0.03 10^{-4}	1 ± 0.2 10^{-5}	6.49 ± 0.5 10^{-4}	1.19 ± 0.0002 10^{-4}	6.22 ± 0.1 10^{-5}
D_{16}	Density of active sites	(mol m^{-2})	6.4 ± 1.5 10^{-6}	4.57 ± 0.05 10^{-7}	9.84 ± 1 10^{-6}	4.33 ± 0.009 10^{-7}	1.33 ± 0.03 10^{-6}

Value ±95% confidence interval. F-value for significance of the regression = 871.1; F tabulated value = 3.36.

complete range of experimental conditions over each of the two catalysts, despite the limited number of adjustable parameters. Furthermore, the outlet molar fractions of each of the C_2 products and carbon oxides as well as those of water, not shown in Fig. 3, were adequately simulated by the model.

In line with the previous work [5] the maximum absolute value among the binary correlation coefficients amounted to 0.85 and occurred between the reaction enthalpy of methane hydrogen abstraction D_1 and the active site concentration D_{16}. Such a value allows concluding that there is no significant correlation between the adjustable parameters. The high F value for the global significance of the regression, amounting to 870, illustrates the model's capability of adapting itself to the experimental data.

Figs. 1 and 2 compare the simulated conversions and product selectivities to the respective experimental values measured at different catalyst temperatures. The model clearly adequately reproduces the methane and oxygen conversions as well as the selectivities to C_2 products and carbon oxides over the LaSr/CaO and NaMnW/SiO_2 catalysts giving confidence in the constructed mechanism and the corresponding model parameters. The parameter estimates obtained for the catalyst descriptors are reported in Table 4. Their values are physically realistic, since they lie within literature reported constraints, as mentioned in Section 3, and are also statistically significant, see Table 4. The respective catalyst descriptor values corresponding to Sr/La_2O_3 and (Sn-)Li/MgO [5] are provided alongside for reference. The values presented in Table 4 highlight the different physicochemical properties of the five investigated catalysts and explain their distinct OCM performances, as illustrated in Table 3, see also the next section.

3.3. Interpretation and quantification of the experimental observations

As mentioned in Section 3 and elaborately described in our previous work [5] the methane hydrogen abstraction reaction enthalpy, D_1, determines the hydroxyl chemisorption enthalpy to a large extent. The hydrogen abstraction from methane appears to be highly endothermic in the case of the Li-MgO as well as of the Na-Mn-W/SiO_2 catalyst. Correspondingly, hydroxyls are less stable on these catalysts, that is their chemisorption heat is relatively less negative and, within the range of the catalyst descriptor values presented in Table 4, this was found to lead to a decrease of heterogeneously catalyzed methane conversion. The positive difference in the activation energies between the forward and the backward direction of the methane hydrogen abstraction step increases with the endothermicity, slowing down the methane conversion. Furthermore, the active site concentration (D_{16}) on these two catalysts is much lower than in the case of Sr/La_2O_3, La-Sr/CaO and Sn-Li/MgO catalysts, implying the limited contribution of the catalytic reactions to the overall OCM reaction rate over Na-Mn-W/SiO_2 and Li-MgO. These findings reveal the intrinsic reason for the low activity of Na-Mn-W/SiO_2 and Li-MgO catalysts illustrated in Table 4.

The catalyst descriptor values presented in Table 4 provide an adequate explanation for the low activity yet simultaneously high selectivity to C_2 products attained with the NaMnW/SiO_2 catalyst. Indeed, this catalyst exhibits the least negative oxygen chemisorption heat, see D_2 in Table 4, which indicates weaker bonding of atomic oxygen to the NaMnW/SiO_2 catalyst surface and, hence, lower contribution of the catalytic reaction network to the overall OCM reaction, since atomic oxygen is involved in a large number of catalytic steps [5]. This effectively slows down methane activation on NaMnW/SiO_2, yet it also limits surface CO_2 formation. The surface production of carbon dioxide is further limited by the decreased oxidation rate of methyl radicals induced by their low sticking coefficient on the surface of the NaMnW/SiO_2 catalyst, see D_{11}, Table 4.

The methane hydrogen abstraction reaction enthalpy, that is D_1, see Table 4, allows explaining the higher activity of Sr/La_2O_3 compared to that of LaSr/CaO under the employed OCM reaction conditions. As can be seen in Table 4, Sr/La_2O_3 exhibits a less endothermic Eley-Rideal methane H-atom abstraction step, D_1. The corresponding hydroxyl chemisorption heat on the Sr/La_2O_3 surface was calculated equal to 278 kJ/mol [5], while for LaSr/CaO the same was limited to 257 KJ/mol. Differences in oxygen chemisorption heat (D_2) and density of active sites (D_{16}) are less critical for explaining the higher activity of Sr/La_2O_3.

As can be readily seen in Table 4 and reported in our previous work [5], the higher activity of Sr/La_2O_3 compared to that of Sn-Li/MgO is attributed to the higher values for D_2 and D_{16} and the lower D_1. Furthermore, Sn-Li/MgO exhibits a higher selectivity to C_2 products than LaSr/CaO due to the correspondingly lower oxygen chemisorption heat (D_2) and the lower value for methyl radical sticking coefficient on its surface (D_{11}). However, a comparison between LaSr/CaO and Sn-Li/MgO catalyst in terms of methane activation is not straightforward. The latter catalyst exhibits a lower methane H-atom abstraction reaction enthalpy, D_1, yet the oxygen chemisorption heat, D_2, and the density of active sites, D_{16}, on its surface are lower than those of the Sn-Li/MgO catalysts.

Given the differences in operating conditions used in the determination of the OCM kinetics, an unequivocal comparison among the various catalysts is only feasible via microkinetic modelling. For this purpose, microkinetic model simulations have been performed at the operating conditions investigated for the Sr/La_2O_3 catalyst. As shown in Fig. 4, the methane conversion over Sr/La_2O_3 catalyst is simulated approximately 2, 5 30 and 33 times higher than over the La-Sr/CaO, Sn-Li/MgO, Na-Mn-W/SiO_2 and Li/MgO catalysts, respectively, under identical operating conditions.

At a space time equal to 0.35 kg s $mol^{-1}{}_{reactants}$, Sr/La_2O_3 and Li/MgO exhibit a similar selectivity to C_2 products amounting to 25% approximately, with the former catalyst being much more active. A much higher C_2 selectivity, amounting to 80% is simulated for the Na-Mn-W catalyst, irrespective of the applied space time, under the investigated conditions. As mentioned before, this can be assigned to the low values for the oxygen chemisorption heat and methyl radical sticking coefficient obtained for this catalyst, see Table 4. Sn-Li/MgO exhibits the second highest selectivity to C_2 products after Na-Mn-W/SiO_2, followed by Sr-La/CaO catalyst.

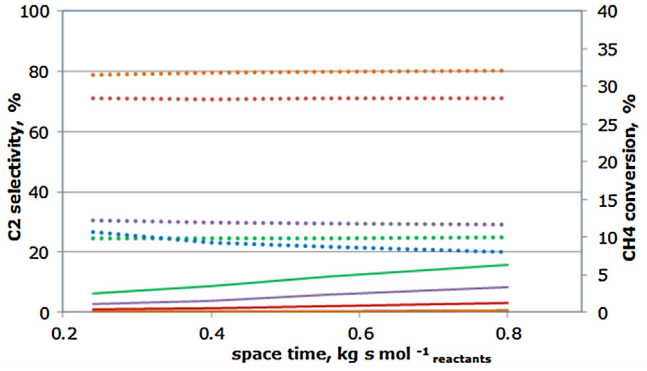

Fig. 4. Simulated methane conversion (full lines) and C_2 selectivity (dotted lines) vs. space time; (green) Sr/La_2O_3; (purple) La-Sr/CaO; (red) Sn-Li/MgO; (orange) Na-Mn-W/SiO_2; (blue) Li/MgO. Operating conditions: T = 1023 K, p = 190 kPa, $CH_4/O_2 = 4$, dilution: 80%. Simulation results were obtained with the model described in section 2 and the values of catalyst descriptors listed in Table 4. Note that because of the differences in operating conditions used during experimental data acquisition, no observed values are reported in this figure. (For interpretation of the references to colour in this figure legend, the reader is referred to the web version of this article.)

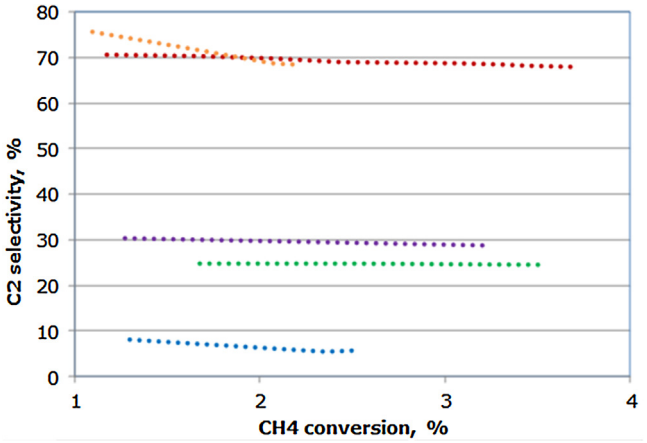

Fig. 5. Simulated C_2 selectivity vs. CH_4 conversion. (green) Sr/La_2O_3; (purple) La-Sr/CaO; (red) Sn-Li/MgO; (orange) Na-Mn-W/SiO_2; (blue) Li/MgO. Operating conditions: T = 1023 K, p = 190 kPa, $CH_4/O_2 = 4$, dilution: 80%. Simulation results were obtained with the model described in section 2 and the values of catalyst descriptors listed in Table 4. Note that because of the differences in operating conditions used during experimental data acquisition, no observed values are reported in this figure. (For interpretation of the references to colour in this figure legend, the reader is referred to the web version of this article.)

The C_2 selectivity as a function of the methane conversion is presented in Fig. 5 to allow a better comparison among the investigated catalysts as a function of the C_2 selectivity. As clearly seen at OCM operating conditions that lead to similar CH_4 conversion, that is around 1–2%, by employing the microkinetic model, the five catalysts are ranked with respect to C_2 selectivity as follows from high to low:

Na-Mn-W/SiO_2 ~ Sn-Li/MgO > La-Sr/CaO > Sr/La_2O_3 > Li/MgO.

4. Conclusions

The present OCM microkinetic model including catalyst descriptors enables the generic description of OCM reaction performances on 5 different catalysts belonging to 4 families based on a single reaction network, irrespective of the operating conditions at which the catalytic performance has been evaluated. The applicability of the model was extended from alkali magnesia catalysts represented by Li/MgO and Sn-Li/MgO and alkaline earth lanthana catalysts represented by Sr/La_2O_3 to two more catalyst families, that is rare earth-promoted alkaline earth calcium oxide catalysts, represented by LaSr/CaO, and a Na-Mn-W/SiO_2 catalyst. The agreement between simulated and experimental conversions and selectivities on all five investigated catalysts for the complete range of experimental conditions was adequate.

The Sr/La_2O_3 catalyst was found to be the most active while Na-Mn-W/SiO_2 proved to be the most selective catalyst towards C_2 products. The above analysis showed that the ideal OCM catalyst should exhibit a low reaction enthalpy of methane H-atom abstraction and high active site density, descriptors which lead to high activity as in the case of Sr/La_2O_3, and low methyl radical sticking coefficient, thus favouring the C_2 selectivity as in the case of Na-Mn-W/SiO_2. Regarding the oxygen chemisorption heat, it was shown that a high value of this descriptor e.g., on Sr/La_2O_3 promotes catalyst activity but limits C_2 selectivity, whereas the opposite effect is induced with a low value, e.g., on Na-Mn-W/SiO_2. Because of these conflicting trends an optimal mediocre value is expected for the ideal catalyst. A microkinetic model including catalyst descriptors is ideally suited to provide guidelines for the development of optimal catalytic systems, the adequate translation of the optimal catalyst descriptor values into a corresponding catalyst synthesis recipe being a critical aspect.

Acknowledgements

This paper reports work undertaken in the context of the project "OCMOL, Oxidative Coupling of Methane followed by Oligomerization to Liquids". OCMOL is a Large Scale Collaborative Project supported by the European Commission in the 7th Framework Programme (GA n°228953). For further information about OCMOL see: http://www.ocmol.eu or http://www.ocmol.com.

The research leading to these results has also received funding from the European Research Council under the European Union's Seventh Framework Programme (FP7/2007-2013)/ERC grant agreement n° 615456 *i*-CaD.

References

[1] G.E. Keller, M.M. Bhasin, J. Catal. 73 (1982) 9.
[2] B.Z.D. Noon, S. Senkan, J. Nat. Gas Sci. Eng. 18 (2014) 406–411.
[3] B. Beck, V. Fleischer, S. Arndt, M.G. Hevia, A. Urakawa, P. Hugo, R. Schomäcker, Catal. Today 228 (2014) 212–218.
[4] M.B.L. Mleczko, Fuel Process. Technol. 42 (1995) 217.
[5] V.I. Alexiadis, J.W. Thybaut, P. Kechagiopoulos, M. Chaar, A. Van Veen, M. Muhler, G.B. Marin, Oxidative coupling of methane: catalytic behaviour assessment via comprehensive microkinetic modelling, Appl. Catal. B (2013).
[6] J. Sun, J.W. Thybaut, G.B. Marin, Microkinetics of methane oxidative coupling, Catal. Today 137 (2008) 90–102.
[7] P. Kechagiopoulos, J.W. Thybaut, G.B. Marin, Ind. Eng. Chem. Res. (2013).
[8] M. Khodadadian, M. Taghizadeh, M. Hamidzadeh, Effects of various barium precursors and promoters on catalytic activity of Ba-Ti perovskite catalysts for oxidative coupling of methane, Fuel Process. Technol. 92 (2011) 1164–1168.
[9] Y. Nakisa, G.M.H. Reza, Modeling the oxidative coupling of methane: heterogeneous chemistry coupled with 3D flow field simulation, J. Nat. Gas Chem. 18 (2009) 39–44.
[10] T. Serres, L. Dreibine, Y. Schuurman, Synthesis of enamel-protected catalysts for microchannel reactors: application to methane oxidative coupling, Chem. Eng. J. 213 (2012) 31–40.
[11] P.M. Couwenberg, Q. Chen, G.B. Marin, Irreducible mass-transport limitations during a heterogeneously catalyzed gas-phase chain reaction: oxidative coupling of methane, Ind. Eng. Chem. Res. 35 (1996) 415–421.
[12] P.M. Couwenberg, Q. Chen, G.B. Marin, Kinetics of a gas-phase chain reaction catalyzed by a solid: the oxidative coupling of methane over Li/MgO-based catalysts, Ind. Eng. Chem. Res. 35 (1996) 3999–4011.
[13] L. Olivier, S. Haag, H. Pennemann, C. Hofmann, C. Mirodatos, A.C. van Veen, High-temperature parallel screening of catalysts for the oxidative coupling of methane, Catal. Today 137 (2008) 80–89.
[14] J.W. Thybaut, J.J. Sun, L. Olivier, A.C. Van Veen, C. Mirodatos, G.B. Marin, Catalyst design based on microkinetic models: oxidative coupling of methane, Catal. Today 159 (2011) 29–36.
[15] S. Arndt, T. Otremba, U. Simon, M. Yildiz, H. Schubert, R. Schomacker, Mn-Na2WO4/SiO2 as catalyst for the oxidative coupling of methane. What is really known? Appl. Catal. A: Gen. 425 (2012) 53–61.

[16] J.X. Wang, L.J. Chou, B. Zhang, H.L. Song, J. Zhao, J. Yang, S.B. Li, Comparative study on oxidation of methane to ethane and ethylene over Na2WO4-Mn/SiO2 catalysts prepared by different methods, J. Mol. Catal. A: Chem. 245 (2006) 272–277.
[17] L.J. Chou, Y.C. Cai, B. Zhang, J.Z. Niu, S.F. Ji, S.B. Li, Oxidative coupling of methane over Na-Mn-W/SiO2 catalyst at higher pressure, React. Kinet. Catal. Lett. 76 (2002) 311–315.
[18] L.J. Chou, Y.C. Cai, B. Zhang, J.Z. Niu, S.F. Ji, S.B. Li, Influence of SnO2-doped W-Mn/SiO2 for oxidative conversion of methane to high hydrocarbons at elevated pressure, Appl. Catal. A: Gen. 238 (2003) 185–191.
[19] K. Huang, X.L. Zhan, F.Q. Chen, D.W. Lu, Catalyst design for methane oxidative coupling by using artificial neural network and hybrid genetic algorithm, Chem. Eng. Sci. 58 (2003) 81–87.
[20] W. Zheng, D.G. Cheng, F.Q. Chen, X.L. Zhan, Characterization and catalytic behavior of Na-W-Mn-Zr-S-P/SiO2 prepared by different methods in oxidative coupling of methane, J. Nat. Gas Chem. 19 (2010) 515–521.
[21] W. Zheng, D.G. Cheng, N. Zhu, F.Q. Chen, X.L. Zhan, Studies on the structure and catalytic performance of S and P promoted Na-W-Mn-Zr/SiO2 catalyst for oxidative coupling of methane, J. Nat. Gas Chem. 19 (2010) 15–20.
[22] V.R. Choudhary, S.A.R. Mulla, V.H. Rane, Surface basicity and acidity of alkaline earth-promoted La2O3 catalysts and their performance in oxidative coupling of methane, J. Chem. Technol. Biotechnol. 72 (1998) 125–130.
[23] Q. Chen, P.M. Couwenberg, G.B. Marin, The oxidative coupling of methane with cofeeding of ethane, Catal. Today 21 (1994) 309–319.
[24] Z.M. Gao, Y.Y. Ma, Direct oxidation of methyl radicals in OCM process deduced from correlation of product selectivities, J. Nat. Gas Chem. 19 (2010) 534–538.
[25] Y.S. Su, J.Y. Ying, W.H. Green, Upper bound on the yield for oxidative coupling of methane, J. Catal. 218 (2003) 321–333.
[26] A.B. Mhadeshwar, H. Wang, D.G. Vlachos, Thermodynamic consistency in microkinetic development of surface reaction mechanisms, J. Phys. Chem. B 107 (2003) 12721–12733.
[27] O.V. Krylov, Catalytic reactions of partial methane oxidation, Catal. Today 18 (1993) 209–302.
[28] J.A. Dumesic, D.F. Rudd, The Microkinetics of Heterogeneous Catalysis, American Chemical Society, Washington, DC, 1993.
[29] N. Schumacher, A. Boisen, S. Dahl, A.A. Gokhale, S. Kandoi, L.C. Grabow, J.A. Dumesic, M. Mavrikakis, I. Chorkendorff, Trends in low-temperature water-gas shift reactivity on transition metals, J. Catal. 229 (2005) 265–275.
[30] A. Michaelides, Z.P. Liu, C.J. Zhang, A. Alavi, D.A. King, P. Hu, Identification of general linear relationships between activation energies and enthalpy changes for dissociation reactions at surfaces, J. Am. Chem. Soc. 125 (2003) 3704–3705.
[31] H.H. Rosenbrock, An automatic method for finding the greatest or least value of a function, Comput. J. 3 (1960) 175–184.
[32] P.T. Boggs, J.R. Donaldson, R.H. Byrd, R.B. Schnabel, Odrpack &minus, Software for weighted orthogonal distance regression, ACM Trans. Math. Softw. 15 (1989) 348–364.
[33] V.E. Ostrovskii, Molar heats of chemisorption of gases at metals: review of experimental results and technical problems, Thermochim. Acta 489 (2009) 5–21.
[34] J. Majzlan, L. Mazeina, A. Navrotsky, Enthalpy of water adsorption and surface enthalpy of lepidocrocite (gamma-FeOOH), Geochim. Cosmochim. Acta 71 (2007) 615–623.